Title
MONTE CARLO STUDIES OF ALPHA-ACCOMPANIED FISSION

Author
Radi, H.M.A.

Publication Date
1982

LBL-13901
Preprint

Lawrence Berkeley Laboratory
UNIVERSITY OF CALIFORNIA

Submitted to Physical Review C

MONTE CARLO STUDIES OF ALPHA-ACCOMPANIED FISSION

Hafez M.A. Radi, John O. Rasmussen, Raul Donangelo,
Luiz F. Canto, and Luiz F. Oliveira

January 1982

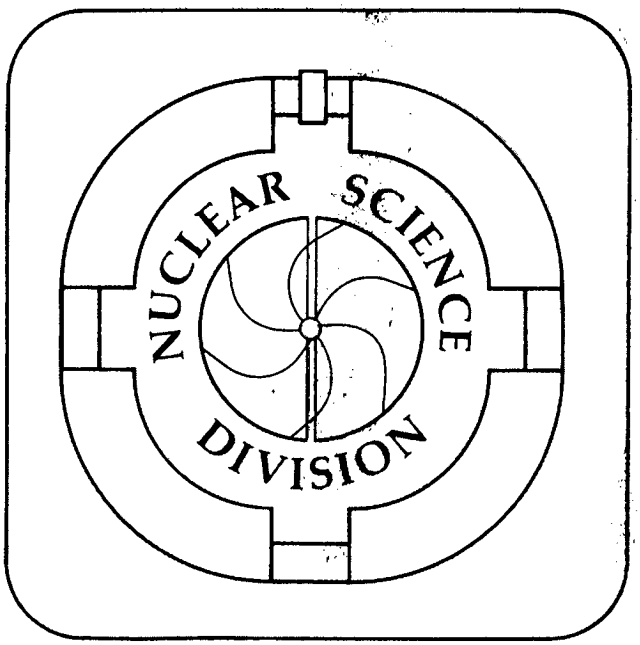

Prepared for the U.S. Department of Energy under Contract W-7405-ENG-48

DISCLAIMER

LBL-13901

Monte Carlo Studies of Alpha-Accompanied Fission

Hafez M.A. Radi
Nuclear Science Division, Lawrence Berkeley Laboratory
University of California, Berkeley, CA 94720 and
Physics Department, Kuwait University, Kuwait

and

John O. Rasmussen
Department of Chemistry, University of California, Berkeley
and Nuclear Science Division, Lawrence Berkeley Laboratory
University of California, Berkeley, CA 94720

and

Raul Donangelo, Luiz F. Canto, and Luiz F. Oliveira
University Federal do Rio de Janeiro, Brazil

Abstract:

To compare with the wealth of new data on alpha-accompanied fission of $^{236}U^*$ we have made new trajectory calculations. Initial conditions for several parameters were selected from Gaussian distributions by the Monte Carlo method and about 15,000 trajectories were run for alpha source at the electrostatic saddle point. Momentum and energy are fully conserved in the three-body problem, though the usual point charge approximation without nuclear forces was used. The main calculations center the alpha source at the electrostatic saddle. General agreement with experiment is remarkable including even the appearance of low-energy secondary peaks at large angles. Effects of shifting the source from the saddle point toward either fragment are studied, running an additional 15,000 trajectories for each of two shifts. Both the satellite peak phenomena and the angular distribution indicate the need for a small shift of source toward the light fragment.

Keyword abstract:
NUCLEAR REACTIONS. Alpha accompanied thermal neutron ternary fission $^{235}U(n,f)$. Monte Carlo theory; trajectory calculations; α-particle angular and energy distributions.

I. Introduction

It has been known that both spontaneous[1-3] and induced[4-6] fission exhibit a ternary branch of a few tenths of a percent. Usually the third charged particle is an alpha particle but with several other rarer species observed. One of the factors impelling recent experiments[7-9] and theoretical[10-22] research on alpha-accompanied fission (hereafter abbreviated to LRA fission, for "long-range-alpha" following Guet et al.[8]) is the possibility of probing the role of the configuration and dynamics of the fissioning nucleus at scission, the viscosity, and the division of energy between ordered and random motion.

The state of knowledge a few years ago was reviewed by Vandenbosch and Huizenga[24]. Since that time there have been significant new studies[8,21].

A notable feature of LRA fission is the sidewise angular distribution of alphas, slightly inclined toward the light fragment ($<\theta_{\alpha L}>$ ranges from 81° for $^{236}U^*$ to 84° for ^{252}Cf). The most probable alpha energies range around 16 MeV for ^{236}U.

Early studies[10-12] with trajectory calculations gave a general understanding that the alphas are evidently emitted from the neck region around the time of scission. The side-peaked angular distributions are a consequence of Coulomb focusing in the field of the two fission fragments. The mean alpha energy is sensitive to initial conditions. For example, if the alpha particle were initially placed at rest at the saddle point of the electrostatic potential from the fission fragments, it would experience virtually no acceleration (a slight amount to the extent that the charge-to-mass ratios of the fission fragments are not identical). On the other hand, the upper limit of alpha energy would be reached if the fission fragments remained fixed at their scission point distance, D. As an estimate for $^{236}U^*$ take $Z_L = 38$, $Z_H = 54$, and D = 17 fm with the alpha starting from

the electrostatic saddle with initial kinetic energy E_i. In this limiting case the final alpha energy would be E_i + 30.93 MeV. Experimental values of the mean alpha energy are about half this limiting value (for $E_i \approx 0$).

The various parameters specifying initial conditions evidently cannot be uniquely determined by the ternary fission data. Thus, we have made our Monte Carlo studies imposing an uncertainty principle constraint on the initial position and momentum distributions of the alpha particle, the fragment's separation distance. Furthermore, we have fixed the value of initial fission fragment kinetic energy based on the Negele et al. calculations[19], but conservation of momentum of the whole system produces an uncertainty on these initial kinetic energies.

II. General Description of the Model

The geometrical view of the initial condition of the light fragment, heavy fragment, and α-particle is shown in Fig. 1. The process is viewed in the center of mass system (which is also essentially the lab system for thermal neutron fission). The two fragments are at a distance D apart and with masses m_L and m_H (from here on the subscripts L and H will indicate light and heavy fragments, respectively). The alpha particle is in a plane at a distance d from the center of the light fragment and at a distance R_c from the point of intersection of this plane with the line joining the center of the two fragments. In Fig. 1 Cartesian coordinates (xyz) are constructed to represent the center of mass of the light fragment, heavy fragment, and the α-particle. The light and heavy fragments have velocities $\vec{V}_L$ and $\vec{V}_H$, respectively, and they are mostly pointed toward left and right (we will point out later the deviation due to recoil effects or strict conservation of 3-body momentum). The α-particle has velocity $\vec{v}_\alpha$ and could be directed anywhere. The initial positions and velocities of light fragment, heavy fragment, and α-particle viewed from the center of mass are generally written as

$$\vec{r}_j^{(i)} = x_j^{(i)} \hat{e}_x + y_j^{(i)} \hat{e}_y + z_j^{(i)} \hat{e}_z \quad ,$$

$$\hat{v}_j^{(i)} = v_{xj}^{(i)} \hat{e}_x + v_{yj}^{(i)} \hat{e}_y + v_{zj}^{(i)} \hat{e}_z \quad , \qquad (j = L,H,\alpha) \tag{1}$$

The components of these two equations are presented in table 1. In this table the initial z-coordinates of the three particles are zero. This is done first by letting the alpha particle have initial coordinates y' and z', so $R_c = [y'^2 + z'^2]^{1/2}$, and rotating the system so that $y' = R_c$. Also in the same table the velocity of the α-particle is in xyz coordinates. Since this velocity is going to be chosen at random, we modify the two fragments' velocities so as to constrain the total momentum of the system to zero with respect to the center of mass.

III. Dynamics of the Model

We shall be concerned in this section with the classical solution for α-particle and two charged fragments (three-body problem). Figure 2 shows the motion of the two fragments and the α-particle with respect to the center of mass at a given time t. This figure represents a later time than Fig. 1, which defined the initial conditions of the problem. The charges are to be considered as point charges. With the use of variables defined in Fig. 2 we can write the requirement of having zero total momentum as

$$\sum_i m_i \dot{\vec{r}}_i = 0 \qquad (i = L,H,\alpha) \tag{2}$$

The kinetic energy of the system about the c.m. is

$$E_K = \sum_i \frac{1}{2} m_i (\dot{\vec{r}}_i \cdot \dot{\vec{r}}_i) \qquad (i = L,H,\alpha) \tag{3}$$

The potential energy of the system is simply the pure monopole-monopole Coulomb potential energy of the interacting three particles and written as

$$V_{pot.} = \sum_{\substack{i,i \\ i\neq j}} \frac{Z_i Z_j e^2}{[(x_i-x_j)^2+(y_i-y_j)^2+(z_i-z_j)^2]^{1/2}} \quad (i,j = L,H,\alpha) \tag{4}$$

The Lagrangian of the system can be constructed and used in Lagrange's equation to get the differential equations of motion. In general, we get differential equations for the light fragment, the heavy fragment, and the α-particle. One can use to advantage the conservation of momentum of the system to decouple, for instance, the heavy fragment variables. This will allow us to solve the differential equation of the light fragment and the α-particle only. As a result of this step, the coupled first-order differential equations of the light fragment and the α-particle are

$$\frac{d\hat{x}_L}{d\hat{t}} = \hat{v}_{xL}$$

$$\frac{d\hat{v}_{xL}}{d\hat{t}} = \frac{Z_L e^2}{m_L c^2 R_o \beta_o^2} [Z_\alpha A_x/A + Z_H B_x/B] \tag{5}$$

and similar equations for y and z,

$$\frac{d\hat{x}_\alpha}{d\hat{t}} = \hat{v}_{x\alpha}$$

$$\frac{d\hat{v}_{x\alpha}}{d\hat{t}} = \frac{Z_\alpha e^2}{m_\alpha c^2 R_o \beta_o^2} [-Z_L A_x/A + Z_H C_x/C] \tag{6}$$

and similar equations for y and z,

where

$$A_x = \hat{x}_L - \hat{x}_\alpha \text{ and similar ones for } A_y \text{ and } A_z, \tag{7a}$$

$$A = (A_x^2 + A_y^2 + A_z^2)^{3/2}, \tag{7b}$$

$$B_x = (1 + m_L/m_H)\hat{x}_L + (m_\alpha/m_H)\hat{x}_\alpha \text{ and similar ones for } B_y \text{ and } B_z, \quad (8a)$$

$$B = (B_x^2 + B_y^2 + B_z^2)^{3/2} , \quad (8b)$$

$$C_x = (m_L/m_H)\hat{x}_L + (1 + m_\alpha/m_L)\hat{x}_\alpha \text{ and similar ones for } C_y \text{ and } C_z, \quad (9a)$$

$$C = (C_x^2 + C_y^2 + C_z^2)^{3/2} , \quad (9b)$$

and where the dimensionless variables, $\hat{x}$, $\hat{v}$, $\hat{t}$, and β_o are given by

$$\begin{aligned} \hat{x} &= x/R_o \\ \hat{v} &= v/V_o \\ \hat{t} &= t/T_o \\ \beta_o &= V_o/c \end{aligned} \quad (10)$$

R_o is taken to be the average of the radii of the two fragments

$$R_o = (R_L + R_H)/2 . \quad (11)$$

Also, V_o is taken to be the average of the speed of the light and heavy fragments before interaction, i.e.,

$$V_o = (V_L^o + V_H^o)/2 , \quad (12)$$

Finally, T_o is taken to be

$$T_o = R_o/V_o , \quad (13)$$

We solve these couplet first order differential equations (Eqs. 5-6) numerically by the Adams Moulton predictor-correct or method. The trajectories are computed as time goes on, keeping track of all three particles (the third one is easily done from conservation of momentum), and checking after a long time for the percentage of change in the α-particle velocity. We wipe out trajectories if the α-particle passes within 0.8 the radius of either of the two fragments.

IV. Random Variations of the Initial Coordinates:

A. The fixed starting initial distribution of the system:

We start by considering a binary fission of ^{236}U only. The reported experimental total fragment kinetic energy is

$$\left\langle E_{KB}(^{236}U)\right\rangle_{\infty} = 168 \pm 4.5 \text{ MeV} \quad , \tag{14}$$

and the average total kinetic energy of the two fragments at scission is given by Negele et al.[19]

$$\left\langle E_{KB}(^{236}U)\right\rangle_{sciss.} = 18.1 \text{ MeV} \quad . \tag{15}$$

For ternary fission, the difference between the total fragment kinetic energy in binary fission and α-accompanied fission (energy balance) is written as

$$\left\langle E_{KT}(^{236}U)\right\rangle_{\infty} = \left\langle E_{KB}(^{236}U)\right\rangle_{\infty} - \left\langle \Delta E(^{236}U)\right\rangle_{\infty} \quad . \tag{16}$$

We take the total fragment kinetic energy for ternary fission of Asghar et al.[7], namely 155.5 ± 0.8 MeV. This gives a difference $\langle \Delta E(U^{236})\rangle_{\infty} \approx 13$ MeV.

At scission, for the α-accompanied fission we apply the same approach

$$\left\langle E_{KT}(^{236}U)\right\rangle_{sciss.} = \left\langle E_{KB}(^{236}U)\right\rangle_{sciss.} - \left\langle \Delta E(^{236}U)\right\rangle_{sciss.} \quad , \tag{17}$$

where

$$\left\langle \Delta E(^{236}U)\right\rangle_{sciss.} \approx 4\text{-}5 \text{ MeV} \quad . \tag{18}$$

Hence

$$\left\langle E_{KT}(^{236}U)\right\rangle_{sciss.} \approx 13 \text{ MeV} \quad . \tag{19}$$

In ternary fission the conservation of energy leads to a relation between the total final scission kinetic energy of the three particles as follows:

$$\left\langle E_{\alpha}\right\rangle_{\infty} + \left\langle E_{KT}(^{236}U)\right\rangle_{\infty} = \frac{Z_L Z_H e^2}{\langle D\rangle} + \frac{Z_{\alpha} Z_L e^2}{\langle d\rangle} + \frac{Z_{\alpha} Z_H e^2}{(\langle D\rangle - \langle d\rangle)} + \left\langle E_{KT}(^{236}U)\right\rangle_{sciss.} + \left\langle E_{\alpha}\right\rangle_{sciss.} \tag{20}$$

The average kinetic energy of α-particle at infinity is measured to be 16 MeV.[24] Following Halpern in our main set of calculations we take the distance d as that of the electrostatic saddle point between the fragments (Fig. 1), and it is related to the distance between the two fragments, D, by

$$d = [\sqrt{Z_H/Z_L} - 1]/[Z_H/Z_L - 1]\, D$$
$$\approx 0.455\ D \text{ for } Z_H = 53 \text{ and } Z_L = 37 \quad , \tag{21}$$

(We later test the saddle-point assumption by shifting the α-position.) If we assume a guessed value for the mean alpha particle kinetic energy at scission then the mean value of the remaining parameters can be calculated from the conservation of energy (Eq. 20). According to Davies et al.[18], the neck radius for scission instability is about 2 Fm. In the appendix we give a derivation of a folded potential for the α-particle, and at the scission neck radius get an alpha kinetic energy of about 5 MeV.

Equation (20) then gives $D_o = \langle D \rangle \approx 21.9$ fm and hence $d_o = \langle d \rangle \approx 9.97$ fm. From conservation of momentum we can also get the two fragment velocities as (for α-particle with zero kinetic energy):

$$V_L^o = 0.013\ c \quad ,$$
$$V_H^o = 0.009\ c \quad . \tag{22}$$

B. Fluctuations in the separation distance D:

The fluctuation in the separation distance D inferred from the width of fission fragment kinetic energy distributions is about 1.0 fm, so a fixed choice of $D = D_o$ is not realistic. We choose D randomly from a Gaussian distribution of the form

$$P(D - D_o) = \frac{1}{\sqrt{2\pi}\,\sigma_D} \exp\left[-\frac{(D-D_o)^2}{2\sigma_D^2}\right] \quad \text{with } \sigma_D \approx 1.0 \text{ fm} \tag{23}$$

Then, there is a

$$Pr(D) = \int_{-\infty}^{D-D_o} dD \frac{1}{\sqrt{2\pi}\,\sigma_D} \exp\left[-\frac{(D-D_o)^2}{2\sigma_D^2}\right]$$

chance that what we choose randomly will be less than or equal $(D - D_o)$. If we let $Pr(D) = \xi$, where ξ is a random variable between 0 and 1, then

$$D = D_o + D_\xi \tag{24a}$$

where

$$D_\xi = \sqrt{2}\,\sigma_D\, erf^{-1}[2\xi - 1] \quad , \tag{24b}$$

and depends on half the width of the Gaussian through σ_D and on the inverse of an error function of $(2\xi - 1)$. Any random choice will give us new value of D and hence new location of the saddle point d_o as it could be evaluated from Eq. (21).

C. Fluctuations of the α-particle position about the saddle point

We follow the uncertainty principle in not starting the α-particle from the saddle point but from a Gaussian distribution around it. Let us consider that the α-particle has an uncertainty around d_o measured by $\sigma_{x'}$ along x'-axis, and given by

$$P(d - d_o) = \frac{1}{\sqrt{2\pi}\,\sigma_{x'}} \exp\left[-\frac{(d-d_o)}{2\sigma_{x'}^2}\right] \quad , \tag{25}$$

where $d-d_o = x'$ in the exponential part of Eq. (25).

Hence (as before),

$$d = d_o + d_\xi \quad , \tag{26a}$$

where $$d_\xi = \sqrt{2}\,\sigma_{x'}\, erf^{-1}[2\xi - 1] \quad . \tag{26b}$$

Of course, the random variable ξ in Eqs. (26) is different from the one used in Eqs. (24) but for simplicity we use the same letter.

Using the same approach, the uncertainty of the α-particle along y' and z' (as shown in Fig. 1) is given in terms of $\sigma_{y'} = \sigma_{z'}$. Then, we can do the same to find y' and z' in a form similar to Eqs. (26). Now, we can compute R_c by

$$R_c = [y'^2 + z'^2]^{1/2} \quad , \tag{27}$$

where

$$y' = \sqrt{2}\,\sigma_{y'}\,\mathrm{erf}^{-1}[2\xi - 1] \text{ and similar equation for } z'. \tag{28}$$

V. Random Variation of the Initial α-velocities

In the previous section we chose the α-particle position about o' from a Gaussian

$$P(x',y',z') = \frac{1}{(2\pi)^3\,\sigma_{x'}\sigma_{y'}^2}\exp\left[-\left(\frac{x'^2}{2\sigma_{x'}^2} + \frac{y'^2+z'^2}{2\sigma_{y'}^2}\right)\right] \tag{29}$$

Using the uncertainty principle, the Fourier transform of this distribution will give the corresponding Gaussian in momentum space as follows:

$$P(P_{x'},P_{y'},P_{z'}) = \frac{1}{(2\pi)^{3/2}\,\sigma_{Px'}\sigma_{Py'}^2}\exp\left[-\left(\frac{P_{x'}^2}{2\sigma_{Px'}^2} + \frac{(P_{y'}^2+P_{z'}^2)}{2\sigma_{Py'}^2}\right)\right] \tag{30}$$

where $$\sigma_{Px'} = \frac{\hbar}{2\sigma_{x'}} \quad , \tag{31}$$

$$\sigma_{P_{y'}} = \frac{\hbar}{2\sigma_{y'}} \quad .$$

The momentum distribution could be written in as a function of velocity distribution (in units of c) as

$$P(\beta_{x'},\beta_{y'},\beta_{z'}) = \frac{1}{(2\pi)^{3/2}}\,\frac{1}{\sigma_{Px'}\sigma_{Py'}^2}\exp\left[-\left(\frac{\beta_{x'}^2}{2S_{x'}^2} + \frac{(\beta_{y'}^2+\beta_{z'}^2)}{2S_{y'}^2}\right)\right] \tag{32}$$

where $$S_{x'} = \frac{\hbar c}{2\sigma_{x'}(m_\alpha c^2)}$$, and a similar one for y. (33)

The standard deviations $\sigma_{x'}$ and $\sigma_{y'} = \sigma_{z'}$ are to be taken as 0.93 fm and 1.3 fm, respectively. The choice of $\sigma_{x'}$ is obtained from the assumption that an estimate of $\sigma_{x'}$ may be of order of magnitude of the root mean square of the radius of the α-particle. The values of $\sigma_{y'} = \sigma_{z'}$ are chosen to be $\sqrt{2}\ \sigma_{x'}$ rather arbitrarily (larger and smaller values of $\sigma_{y'}$ were used, and they remove the agreement between theory and experiment).

VI. Parameter Distributions and Results

In Fig. 3 we plot the initial distributions of several parameters. The top curve is the distribution of D, the fission fragment separation distance at scission. Both the actual histogram and the Gaussian fit are shown. The middle curve gives the distribution of d, the location of the saddle with respect to light fragment; it is computed from each random choice of D and is not separately chosen. The lowest curve gives the off-axis distribution of the initial alpha position, both histogram and computer-smoothed curve shown. This distribution follows from the $\sigma_{y'}$ parameter, which was varied to find optimum agreement as mentioned before. The most probable values of D, d, and R_c are 21.9 fm, 9.97 fm, and about 1.2 fm. The standard deviations (from the Gaussian fit) of D and d are σ_D = 1 fm and σ_d = 1.04, respectively.

The upper part of Fig. 4 shows the initial kinetic energy distribution of the light fragment with most probable value of 7.4 MeV and standard deviation of 0.55 MeV. This energy is not independently chosen but follows from the random choice of alpha initial momenta and the conservation of momentum (Table I). The lower part shows the final distribution and the fitted Gaussian centered at 89.0 MeV with standard deviation 4.2 MeV. This is to be compared with Asghar et al.[7] results, 92.85 ± 0.58 MeV and 9.9 ± 0.05 MeV from Table I of Guet et al.[8] It must be remembered that the experimental values are averaged over all fission mass asymmetries, and our calculations are for a fixed asymmetry. Thus, our narrower dispersion is not unreasonable.

Figure 5 shows the corresponding heavy fragment initial and final distributions, and the same remarks apply. Our total mean kinetic energy of 152.1 MeV to be compared with experimental values of 153.6 ± 3 and 155.5 ± 0.8 MeV of Guet et al.[8] and Asghar et al.,[7] respectively.

Figure 6 displays initial and final distributions of the alpha velocity component parallel to the fission fragment axis. The initial distribution is governed by the dispersion constant $\sigma_{Px'}$, which is tied to $\sigma_{x'}$ by the uncertainty relation. The focusing action of the Coulomb field in narrowing, and shifting toward the light fragment is apparent. Figure 7 shows initial and final distributions of the perpendicular component of alpha velocity. From the cylindrical geometry the initial distribution will be velocity times the Gaussian. Again the width of the distribution is tied to the selected width for the position distribution. The Coulomb acceleration has raised the final mean velocity to more than four times its initial value, and the distribution has slightly broadened with a skew toward lower velocities. From final peak positions in Figs. 6 and 7 the most probable angle can be calculated approximately as $\tan^{-1}(\hat{V}_{yz}/\hat{V}_x)$.

The velocity distributions of Figs. 6 and 7 are combined in Fig. 8 to display initial and final alpha kinetic energy distributions. The initial distribution is nearly a standard Boltzmann distribution with a temperature around 1.5 MeV. The initial alpha velocity distribution we chose is not isotropic. The position uncertainty in either perpendicular direction is taken as about 1.4 times greater than in the parallel direction. Although we did not extensively explore the effect of anisotropy, the final conditions gave much better results than for the isotropic choice. Maybe such positional anisotropy can be rationalized in terms of normal modes of vibration of the system at scission. Certainly we do not imply that we have proved anisotropy

to be required. Since we use the uncertainty principle as a constraint, the positional anisotropy implies a forward-backward anisotropy in initial velocity distribution.

The final kinetic energy distribution averaged over all angles in Fig. 8 is well fit by a Gaussian, although we shall see that individual angle cuts are not. The Gaussian parameters are $\langle E_\alpha \rangle$ = 15.9 MeV and standard deviation σ_{E_α} of 5.1 MeV.

In several figures to follow we have chosen angle and energy intervals as near as possible to figures of Guet et al.[8] Thus, we can better facilitate a careful comparison with their experiments. Our order of presentation also follows theirs. Except in a few cases we have not superposed their data on our graphs, since numerical values of their data were not available to us. Thus, it may be helpful for the reader to have a copy of their article available while examining some of our figures.

Our Fig. 9 is analogous to their fig. 3, giving alpha energy distributions for fixed angles, the interval being ±2.5° from the stated angle. The angle is measured from the direction of the light fragment. We show the event number histograms and computer-fitted Gaussians. The cross comparison of the main features, Gaussian centroid and width, are best made on Fig. 10, but we first discuss shapes in Fig. 9. One should bear in mind that our Monte Carlo calculation is for fixed mass asymmetry, and their presentation of data in fig. 3 is for all asymmetries. For the angles 68° through 88° we get fairly good unskewed Gaussian fits. For 93° and larger angles we see a secondary peak develop at lower energies. In their fig. 3 data the secondary peak at lower energies is manifested at both large and small angles. Guet et al.[21] in their own Monte Carlo study have stated that the low-energy component at small angles comes from trajectories starting near

the light fragment heading toward the heavy fragment and backscattering from it. We shall later show our tests shifting the alpha source from the saddle toward either of the fragments.

Our Fig. 10 appears analogous to their fig. 4 but actually is a comparison with their fig. 6 curves for the particular mass asymmetry range we actually calculated, namely, $A_L = 95$, $Z_L = 37$. The lower curve gives the experimental mean energy as a function of angle. We must sound a note of caution in these comparisons, since the basis of getting $\langle E_\alpha \rangle$ is somewhat different. Guet et al.[8] state for their fig. 6, with which we compare, and their fig. 4 that "the average is taken from 7.5 MeV to the maximum measured energy," whereas for their similar earlier fig. 5 $\langle E_\alpha \rangle$ is "output of a least squares Gaussian fit above 13 MeV".

Since the experimental distributions develop low energy peaks at large and small angles, the average or mean energy will not always correspond to the most probable. For our theory we make at each angle a simple least squares fit of all our events to a single symmetric Gaussian and plot its parameters in Fig. 10. The points show our values for the main calculations.

Our mean energy points show the same concave-upward shape but do not rise as do the data for small angles. On the Monte Carlo theory calculation of Guet et al.[21] they did reproduce the upward energy trend at small angles. Since a major difference of our two Monte Carlo studies is their use of uniform distribution along the neck and our use of Gaussian at the saddle point, it would seem that the high energy shift at low angles comes from alphas originating away from the saddle. Our standard deviations are uniformly somewhat larger than experiment.

As one sees from Fig. 11 our theoretical all-energy angular distribution (histogram) perfectly matches the Guet et al. data[8] (dots) around the

maximum. However, the match is less good in the wings of the curve. Our Fig. 11 is analogous to their Fig. 9. However, note that their Fig. 9 counts only alphas $E_\alpha > 7.5$ MeV, and this would seem to affect mainly small angle data as can be seen from Fig. 11. Taking their cut-off into account makes for greater disagreement with our points. However, in our final section we explore shifting the alpha source position and see that a shift toward the light fragment acts to correct this angular distribution mismatch.

In Fig. 12 we show, in analogy to their fig. 10, the angular distributions of alphas for fixed energy intervals. Our plot shows absolute number of Monte Carlo events per bin, whereas their experimental figure appears to have renormalized the angular distribution within each energy bin. The highest two energy intervals have the broadest angular distributions in both experiment and theory. In the other four boxes the most probable angle agrees in all cases, except they show for E_α = 11-13 MeV 78° and 83° equally probable. The experimental and theoretical widths seem quite comparable.

As mentioned earlier, we wished specially to investigate shifting the alpha source along the line of centers. Figure 13 shows the distribution of a position on the x-axis for the two new calculations (shifted from saddle point). The shifts are arbitrary and amount to about one-third the distance to a fragment surface (considered as a sphere). Our testing of these shifts was prompted by remarks of Guet et al.[21] that the low-energy satellite peaks come from alphas starting well away from saddle. However, the results are more complex than their discussion indicated.

Our Figs. 14 and 15 are energy distributions at fixed angles for the shifts toward light and heavy fragment, respectively. These figures are analogous to Fig. 9 for the saddle-point center. On fig. 14 we see that the shift toward light does not produce any clear double-peaking, but there is a pronounced broadening and shift to low energy for small angles.

The shift toward the heavy fragment produces dramatic double-peaking, as is clear from Fig. 15. This double-peaking is most prominent for the larger angles 88°-98°. For the angle 111° the number of events is small and it is difficult to get useful information. It seems likely for the shift toward heavy fragment that two classes of trajectories can lead to the same final angle. The trajectory that starts sideways experiences a maximal acceleration and gives the upper energy peak. The other class of trajectory must start toward the light fragment and experience a rather larger deflection and time delay in the saddle point region. As it leaves the saddle region, the fission fragments will already have separated and the Coulomb acceleration will be much reduced.

We present in Fig. 16 separate angular distribution plots for the shifted cases. The position shift toward light fragment moves the peak of the angular distribution toward larger angles and vice versa. A small admixture of light-shifted component could improve the angular distribution of Fig. 9. Clearly we would not want to add much of the heavy-shift case, since the angular shift is wrong and the experimental data do not show much of low energy satellites at 88° and 93°. Our unshifted results in Fig. 9 already produce enough satellite strength at 98° and 111°. On the other hand, our unshifted results do not give enough satellite strength at the small angles 68° and 73°. Thus, adding in some of the Fig. 14 results from light shift would help reproduce this feature. We conclude that an alpha source distribution somewhat shifted from saddle toward light fragment might give optimum agreement with experiment down to fine details of satellite structure. In their experimental paper, Guet et al.[8] express doubt about their large angle satellites being alphas, saying they might be hydrogen isotopes. The natural occurrence of satellites in our Monte Carlo work makes the alpha assignment more likely.

VII. Discussion

We believe that our calculations and those of ref. 21 show the adequacy of Monte Carlo work based on the dominant monopole-monopole Coulomb interaction. The refinements of the higher moment interactions explored by Carjan and Leroux[23] remain to be more fully taken into account, but they will require a greater attention to dynamics of large-amplitude nuclear vibrations. Likewise, nuclear forces in the calculation could alter trajectories grazing one of the fragments. It is not always clear from earlier trajectory papers whether energy and momentum were strictly conserved, as we did, or whether the alpha moved in the field of the unperturbed fission fragments. It is hard to say how much difference it makes to take the recoil terms into account.

Without much more study varying parameters of initial conditions it is hard to say how uniquely fixed are the conditions in parameter space. We used a theoretical value of 13 MeV for scission-point fission kinetic energy. It seems unlikely that substantial departures from this value could be compensated by other parameters.

The effect of shifts of α-source from saddle-point toward one or the other fragment we showed to be dramatic. The angular distribution shifts in the opposite way, and double peaks become prominent. We concluded that the best starting conditions might involve a slight shift toward light fragment.

A future goal might well be the formulation of a dynamic model for the initial conditions of alpha and fission fragments and to extend to fragments other than alphas. We hope our work constitutes a step toward these goals.

Acknowledgments

This work was mainly supported by the Division of Nuclear Physics of the Office of High Energy and Nuclear Physics of the U.S. Department of Energy under Contract W-7405-ENG-48. The work had its beginnings at the Universite Federal do Rio de Janeiro in July 1981. One of us (J.O.R.) is grateful for the hospitality and support of Prof. Solange di Barra and her nuclear physics group at UFRJ and to the COPPE program in the Engineering Department.

One of us (H.R.) gratefully acknowledges sabbatical support from Kuwait University and hospitality of the University of California Lawrence Bekeley Laboratory during the course of this work.

We are grateful to Dr. M. Guet for sending many reports, published and unpublished, and large-scale copies of their figures for our use in preparing figures.

Appendix A

Models of Alpha Initial Conditions

Our hope in starting this work was that we could formulate a model that would so constrain the alpha initial conditions that other fission parameters could be determined. It did not prove simple to arrive at a unique prescription for the initial alpha conditions, but we set forth some of the considerations.

We first began working with Swiatecki's[25] simplified dynamic model for heavy-ion fusion, running it for the inverse process, fission. The program calculated fragment separation, fragment kinetic energy, neck diameter, as a function of time. One-body dissipation is built into the equations. One must choose an initial kinetic energy at saddle, usually 1 MeV.

We presumed the perpendicular part of the alpha wave packet would be governed by the potential provided by the neck nucleons. If motion were not too fast, the alpha should adiabaticaly adjust to its ground state in the potential. If motion became fast, i.e. near scission, we thought we might have to apply time-dependent perturbation theory to the alpha wave packet. However, it turns out that the alpha wave packet should be quite stationary in the last stages before scission. To see this let us formulate the nuclear matter density profile across the neck as a Gaussian

$$\rho = \rho_0 \exp\left(-y^2/R_n^2\right) \quad . \tag{A1}$$

We assume a Gaussian potential of range r_0 between neck nucleons and the alpha.

$$V(\vec{r}_\alpha - \vec{r}_n) = V_0 \exp\left(-|\vec{r}_\alpha - \vec{r}_n|^2/r_0^2\right) \tag{A2}$$

After some algebra folding the force and the density distribution we get the following simple expression for the alpha potential

$$V(y) = V_{sat} \frac{R_n^2}{\left[R_n^2+r_o^2\right]} \exp\left[-y^2/(R_n^2 + r_o^2)\right] \quad , \tag{A3}$$

where V_{sat} gives the saturation value of the potential as the neck radius R_n becomes infinite. From arguments based on binding energies of the light α-particle nuclei we estimate V_{sat} as -23 MeV. The range r_o is presumably around the normal nuclear force range of 1.4 fm.

To get the size of the lowest alpha wave function in this inverted Gaussian potential we take the curvature at the minimum and approximate with a harmonic oscillator potential $V \approx V_{min} + (1/2)Cy^2)$, with spring constant C.

$$C = 2\, V_{sat}\, R_n^2\, [R_n^2 + r_o^2]^2[(A_n - 4)/A_n] \quad , \tag{A4}$$

where the last factor, involving nucleon number in the neck, is applied to give a measure of self consistency.

Then the alpha zero-point energy is $E_y = (1/2)\hbar\, (C/m_\alpha)^{1/2}$. There are two perpendicular directions so zero point energy is doubled. Table A1 shows the time evolution of ^{236}U fission into $Z_L = 38$, $A_L = 97$, $Z_H = 54$, $A_H = 139$. That we eventually used other theoretical calculations for initial fragment scission kinetic energy came from discussion with Swiatecki[26]. However, note that the kinetic energy as the neck reaches the unstable 2 fm is numerically about the same as we took from other theory[22].

The remarkable and encouraging feature is that the alpha zero-point energy takes on a nearly constant value near scission. (Recall that Davies et al.[18] say scission instability occurs at a neck radius of about 2.0 fm.) This constancy comes about from two opposing tendencies; namely, as the neck

narrows at first the alpha well becomes narrower but as narrowing reaches the force range, the potential becomes shallower, eventually giving a wider well. The perpendicular direction zero-point energy of ∿5 MeV is reasonable but a good bit higher than the values we eventually chose for optimum Monte Carlo results. Perhaps lower energy and greater position uncertainty come from considering bending modes at scission.

Our original idea was that the alpha zero-point motion along the axis was constrained about the saddle by the gently rising electrostatic potential. Eventually we rather tightly restricted the alpha along the saddle and showed that a shift, especially toward heavy fragment, could not be tolerated.

We believe that the axial position might more be governed by nuclear shell model considerations for a particular pair of fragments. The relative distances of scission and of alpha source from the fragments will depend on the relative deformability of their nuclear shapes, hence the relation of their nuclear numbers to the closed shell or subshell numbers. The dispersion of the axial position would depend on zero-point vibration amplitudes of the fragments in an out-of-phase normal mode.

Thus, further studies concentrating on alpha distributions for particular fission asymmetries could elucidate these ideas.

Table 1. Initial coordinates and velocities of the light fragment, heavy fragment, and α-particle with respect to the center of mass.

j	$x_j^{(i)}$	$y_j^{(i)}$	$z_j^{(i)}$
L	$(m_\alpha/M)\delta x + (m_H/M)D$	$-(m_\alpha/M)R_c$	0
H	$-(m_{LH}/M)\delta\ x - D + d$	$y_L^{(i)}$	0
α	$-(m_{LH}/M)\delta\ x$	$(m_{LH}/M)\ R_c$	0

j	$v_{xj}^{(i)}$	$v_{yj}^{(i)}$	$v_{zj}^{(i)}$
L	$v_L^\circ - \delta V$	$-(m_\alpha/m_{LH})\ v_{y\alpha}^{(i)}$	$-(m_\alpha/m_{LH})\ v_{z\alpha}^{(i)}$
H	$v_H^\circ - \delta V$	$v_{yL}^{(i)}$	$v_{zL}^{(i)}$
α	$v_{x\alpha}^{(i)}$	$v_{y\alpha}^{(i)}$	$v_{z\alpha}^{(i)}$

M is the total mass of the system, m_{LH} is the total mass of the light and heavy fragments, and m_i ($i = L,H,\alpha$) stands for the individual mass.

$\delta x = d - (m_H/m_{LH})D.$

$\delta V = [m_L V_L^o - m_H V_H^o + m_\alpha v_{x\alpha}^{(i)}]/m_{LH}.$

Table A1

Dynamic Calculation of Fission Evolution

Time (0.815×10^{-21} s)	Distance D(fm)	Neck Radius R_n(fm)	Fragment Kinetic Energy (MeV)	Alpha Potential Depth (MeV)	Alpha Zero-point Energy (Mev)
0	10.64		1.000	(saddle)	
3.1	11.98	4.12	0.222	(neck first appears)	
4.0	12.82	3.84	0.654	-10.25	2.34
4.5	13.54	3.58	1.275	-19.90	3.79
5.0	14.56	3.19	2.710	-19.22	4.56
5.2	15.10	2.97	3.798	-18.75	4.84
5.4	15.74	2.70	5.479	-18.04	5.12
5.6	16.52	2.34	8.207	-16.84	5.35
5.7	16.97	2.11	10.23	-15.86	5.37
5.8	17.48	1.82	12.95	-14.37	5.13
5.9	18.05	1.45	16.72	-11.79	3.76

References

1. L.W. Alvarez: as reported by G. Farwell, E. Segre, C. Wiagand, Phys. Rev. 71, 327 (1947)
2. E. Segre, Phys. Rev. 86, 21 (1952)
3. W.J. Swiatecki, Phys. Rev. 100, 937 (1955)
4. R.W. Lamphere, Nucl. Phys. 38, 561 (1962)
5. L. Wilets and D.M. Chase, Phys. Rev. 103, 1296 (1956)
6. J.D. Cramer and J.R. Nix, Phys. Rev. C 2, 1048 (1970) and references therein
7. M. Asghar, C. Carles, R. Chastel, T.P. Doan, M. Ribrag, and C. Signarbieux, Nucl. Phys. A 145, 657 (1970)
8. C. Guet, C. Signarbieux, P. Perrin, H. Nifenecker, M. Asghar, F. Caitucolli, and B. Leroux, Nucl. Phys. A314, 1 (1979)
9. F. Caitucoli, B. Leroux, G. Barreau, N. Carjan, T. Benfoughal, T.P. Doan, F. El Hage, A. Sicre, M. Asghar, P. Perrin, G. Siegert, Z. Phys. A-Atom & Nucl. 298, 219 (1980); M. Debeauvais, J. Tripier, S. Jokic, Z. Todorovic, and R. Antangasijevic, Phys. Rev. C 23, 23 (1981)
10. I. Halpern, Proc. IAEA Symp. Phys. Chem. Fission, Salzburg 2, 369 (1965)
11. Y. Boneh, Z. Fraenkel, and I. Nebenzahl, Phys. Rev. 156, 1305 (1967)
12. I. Halpern, Ann. Rev. Nucl. Sci. 21, 245 (1971)
13. K.T.R. Davies, A.J. Sierk, J.R. Nix, Phys. Rev. C 13 (1976)
14. A. Gavron, Phys. Rev. C 11, 580 (1975)
15. K.T.R. Davies and A.J. Sierk, Jour. Comp. Phys. 18, 311 (1975)
16. J. Blocki, J. Randrup, W.J. Swiatecki, and C.F. Thsang, Ann. Phys. 105, 427 (1977)
17. A.J. Sierk and J.R. Nix, Phys. Rev. C 16, 1048 (1977)
18. K.T.R. Davies, R.A. Managan, J.R. Nix, and A.J. Sierk, Phys. Rev. C 16, 1890 (1977)

19. J.W. Negele, S.E. Koonin, P. Möller, J.R. Nix, and A.J. Sierk, Phys. Rev. C 17, 1098 (1978)

20. H.J. Krappe, J.R. Nix, and A.J. Sierk, Phys. Rev. C 20, 992 (1979)

21. C. Guet, H. Nifenecker, C. Signarbieux, and M. Asghar, Proc. Int. Symp. on Phys. and Chem. of Fission, Jülich, May 1979. IAEA Report SM-241/F13

22. A.J. Sierk and J.R. Nix, Phys. Rev. C 21, 982 (1980)

23. N. Carjan and B. Leroux, Phys. Rev. C 22, 2008 (1980)

24. R. Vandenbosch and J.R. Huizenga, Nuclear Fission, p. 382 (Academic, New York, 1973)

25. W.J. Swiatecki, Physica Scripta 24, 113 (1981).

26. W.J. Swiatecki, Private Communication (1981).

Figure Legends

Fig. 1. Schematic diagram of coordinates at time zero for the alpha-particle, fission-fragment system.

Fig. 2. Schematic diagram of coordinates for the process at later time.

Fig. 3. Initial probability distributions of some parameters. The top curve is the distribution for fragment separation distance D. The middle curve is the x-separation d between alpha and light fragment. The lowest curve is the off-axis distance distribution for the alpha.

Fig. 4. Initial and final kinetic energy distributions of the light fragment.

Fig. 5. Initial and final kinetic energy distributions of the heavy fragment.

Fig. 6. Initial and final distributions of x-component of alpha velocity. Units are V_o (=0.011 c), average mean initial velocity of light and heavy fragment.

Fig. 7. Initial and final distributions of the perpendicular (yz) component of alpha velocity.

Fig. 8. Initial and final alpha kinetic energy distributions.

Fig. 9. Final alpha energy distributions for fixed angles 2.5° of the labeled angle $\theta_{\alpha L}$, the angle between alpha and light fragment final velocity vectors. Alpha source entered at electrostatic saddle point.

Fig. 10. Plots of mean alpha energy (lower) and width (standard deviation, upper) vs angle for a particular fission asymmetry. Points are our theory and solid curve is experiment of ref. 8.

Fig. 11. Final alpha angular distribution (histogram theory--all energies) (dots experiment of ref. 8--energies > 7.5 MeV).

Fig. 12. Alpha angular distribution for fixed energy intervals, theory.

Fig. 13. Initial alpha axial position distributions for two cases studying shifts of source from saddle point.

Fig. 14. Same as Fig. 9 except that alpha source is shifted from saddle toward light fragment.

Fig. 15. Same as Figs. 9 and 14 except that alpha source is shifted from saddle toward heavy fragment.

Fig. 16. Final alpha angular distributions (all energies) for the two source-shift cases.

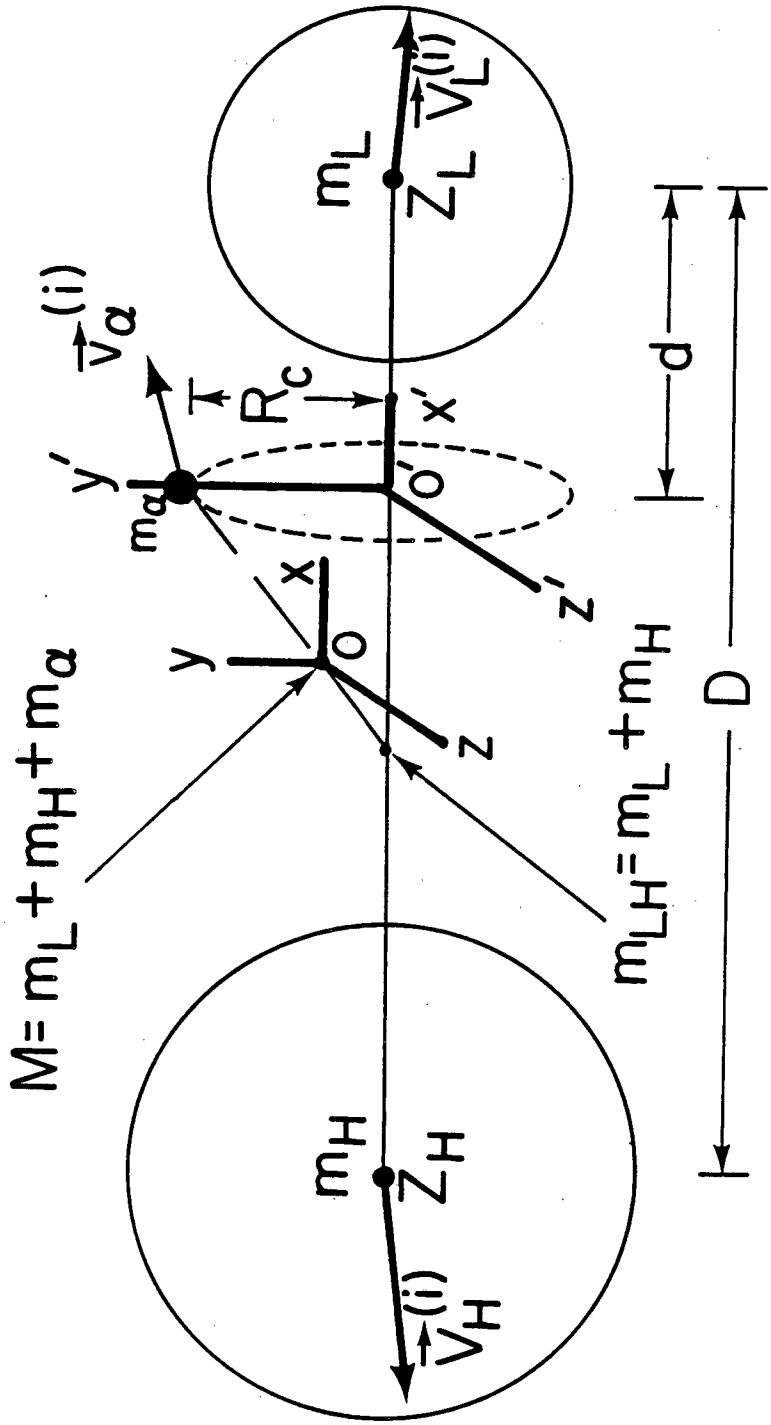

XBL 821-4409

Fig. 1

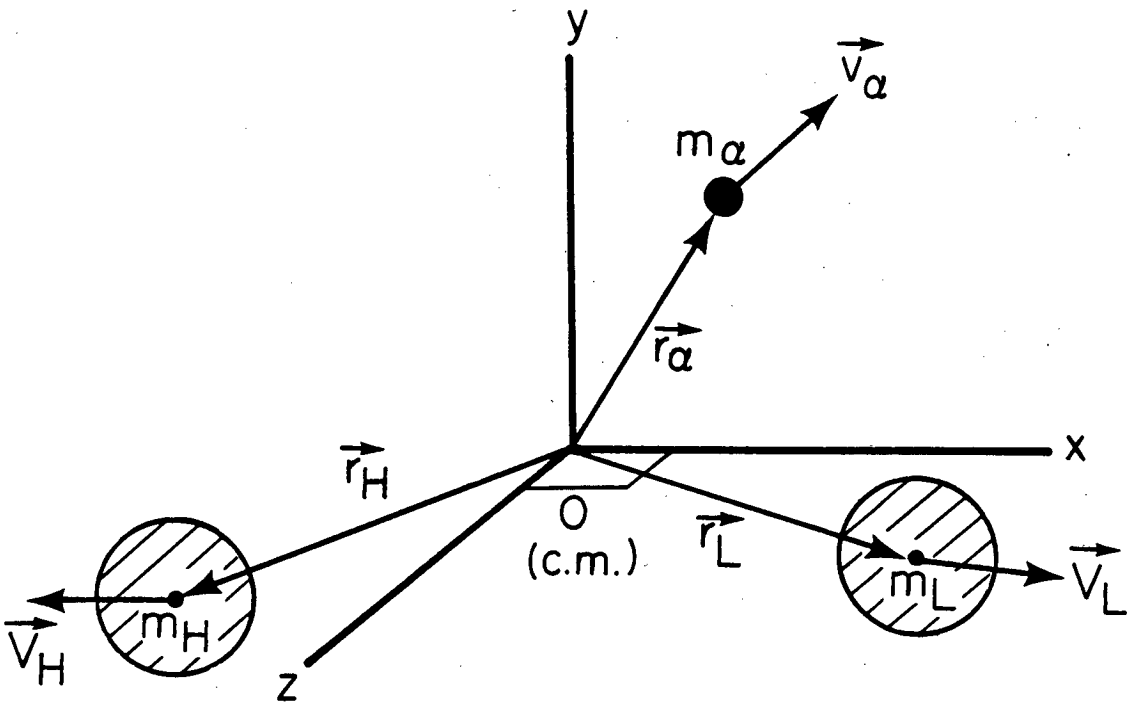

Configuration at time t

XBL821-4410

Fig. 2

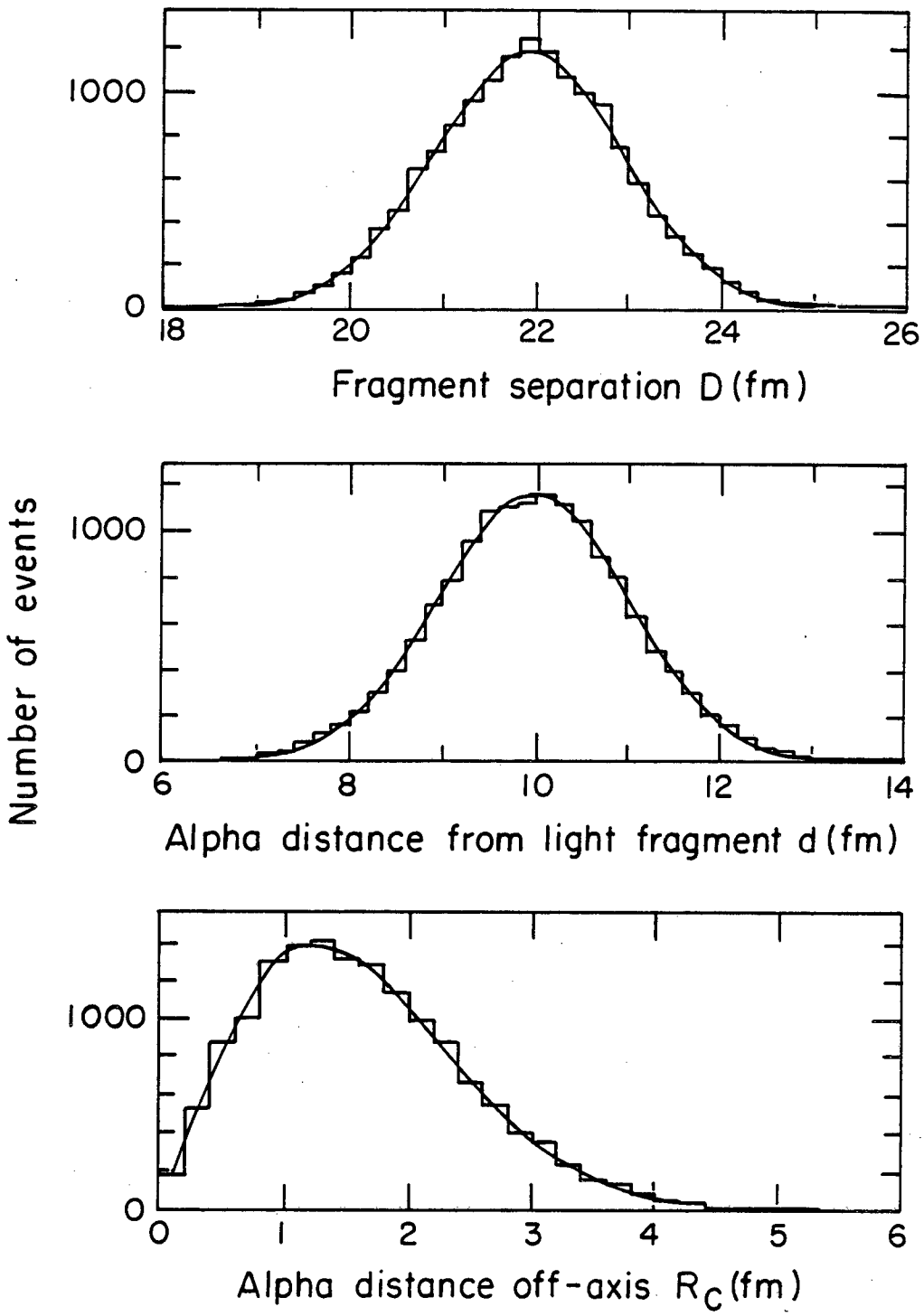
1000
0
18
20
22
24
26
Fragment separation D (fm)
Number of events
1000
0
6
8
10
12
14
Alpha distance from light fragment d (fm)
1000
0
0
1
2
3
4
5
6
Alpha distance off-axis R_C (fm)
XBL 821-4418

Fig. 3

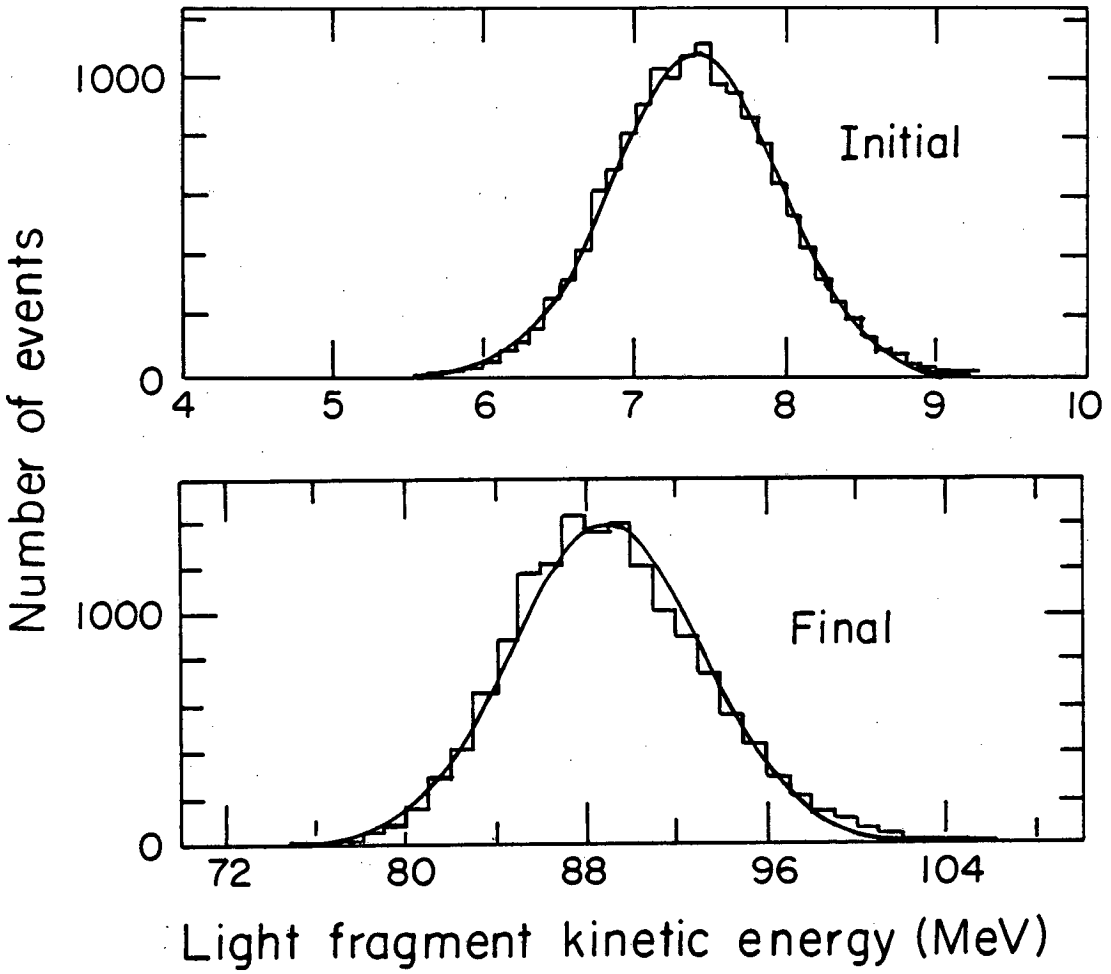
1000
0
Initial
4
5
6
7
8
9
10
Number of events
1000
0
Final
72
80
88
96
104
Light fragment kinetic energy (MeV)
XBL821-4421

Fig. 4

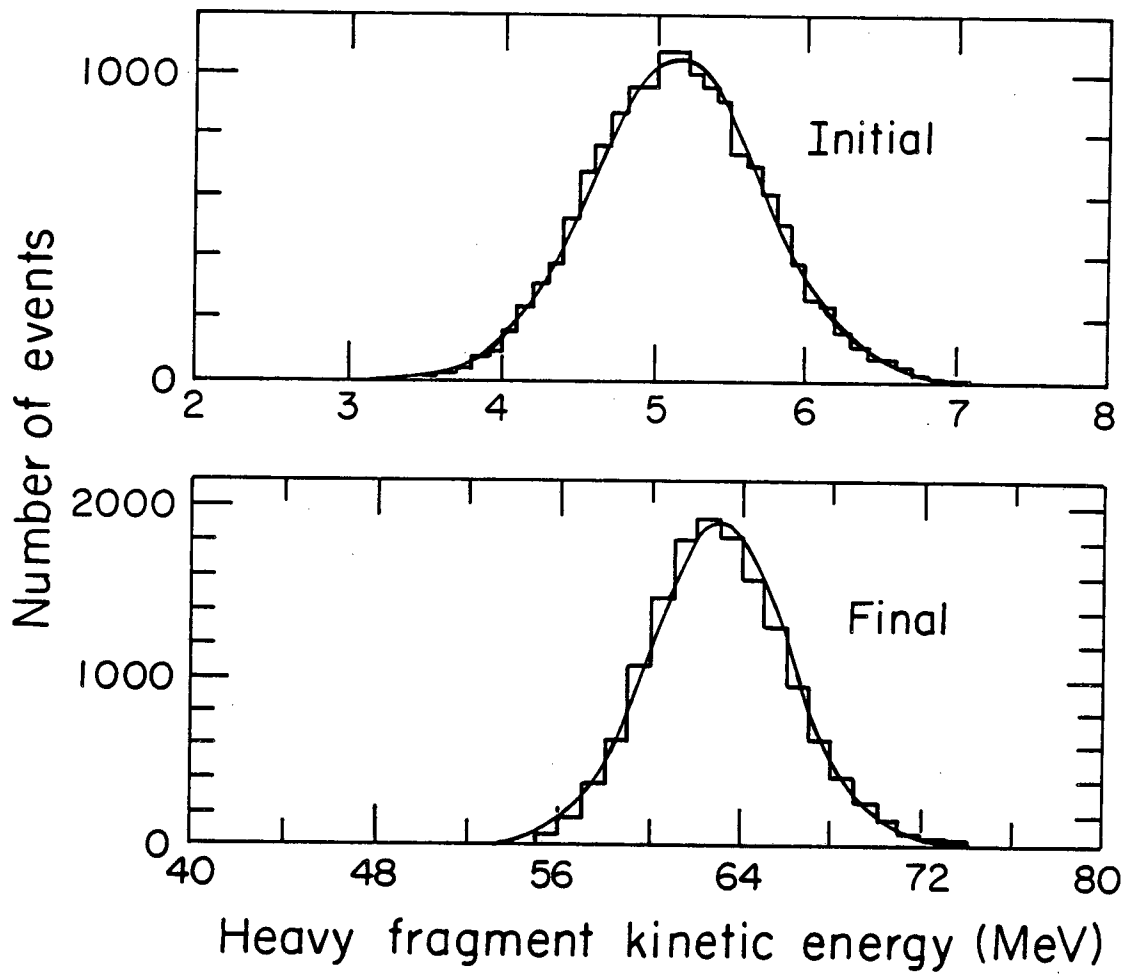

XBL821-4420

Fig. 5

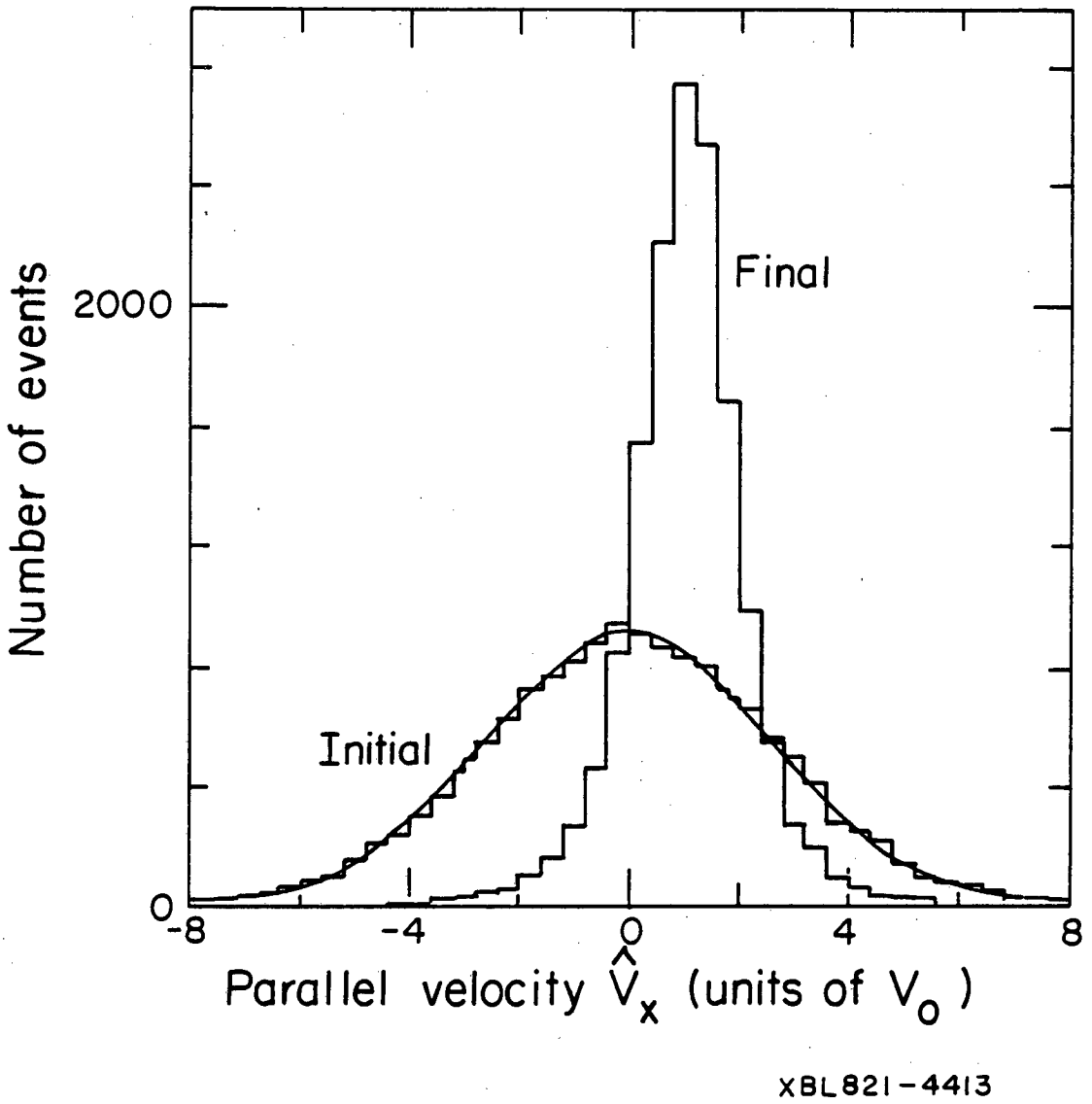
Number of events
2000
0
Final
Initial
-8
-4
0
4
8
Parallel velocity $\hat{V}_x$ (units of V_0)
XBL821-4413

Fig. 6

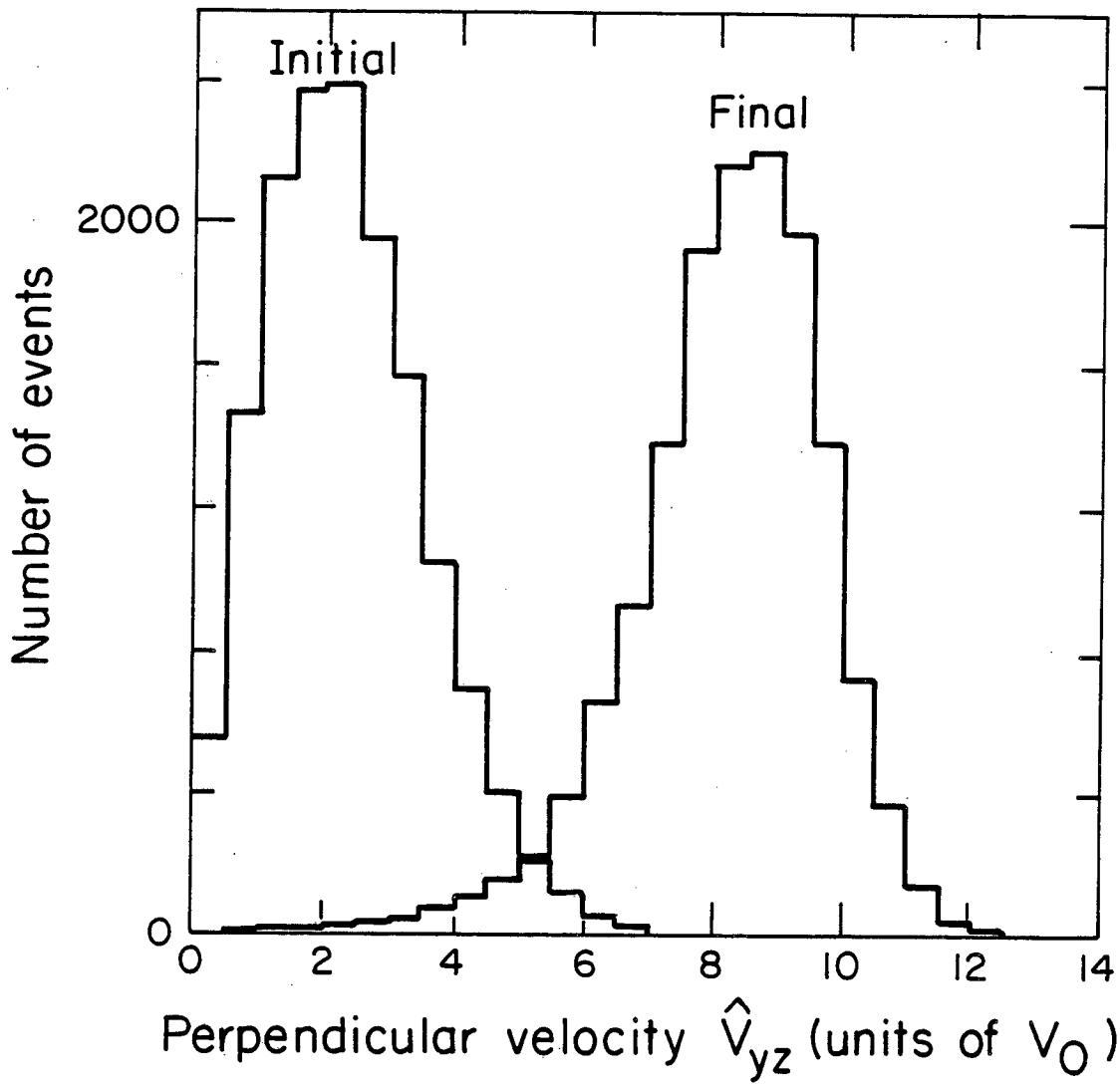

XBL821-4408

Fig. 7

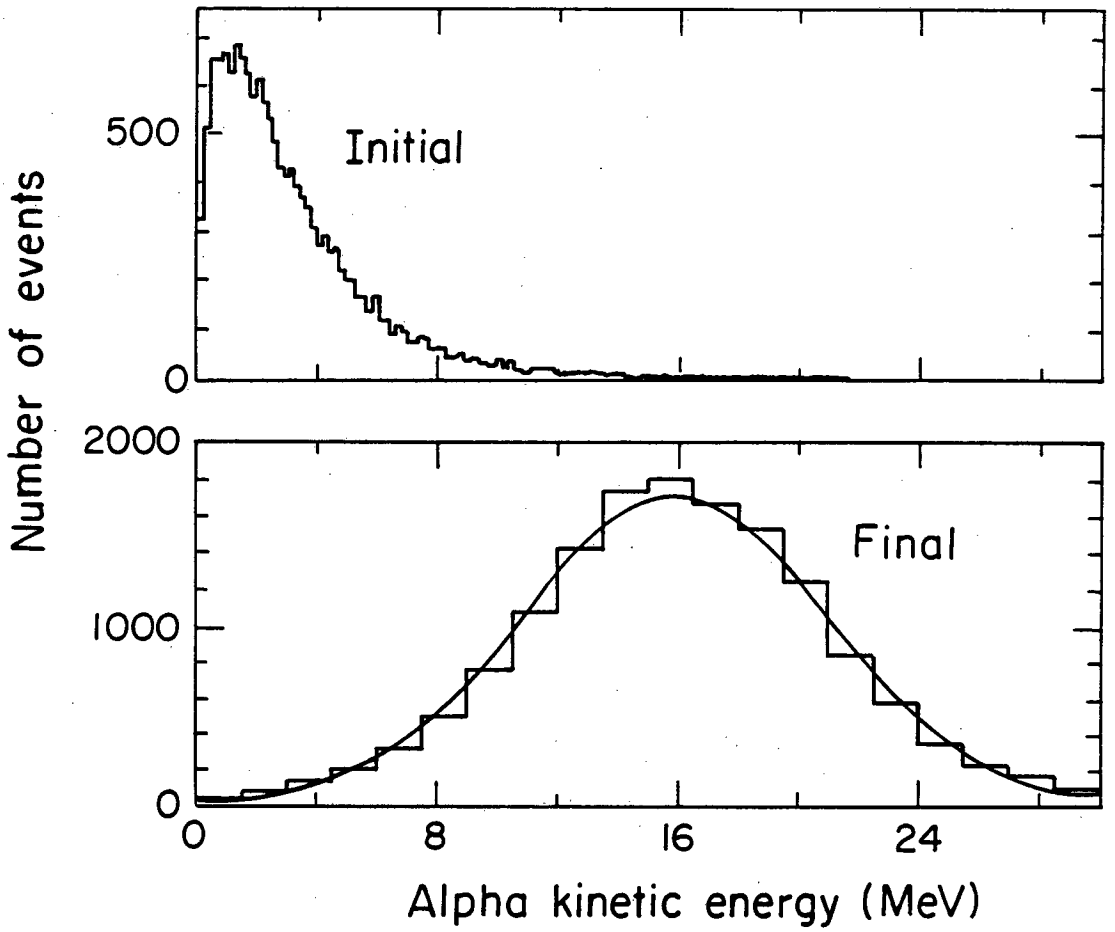

XBL 821-4412

Fig. 8

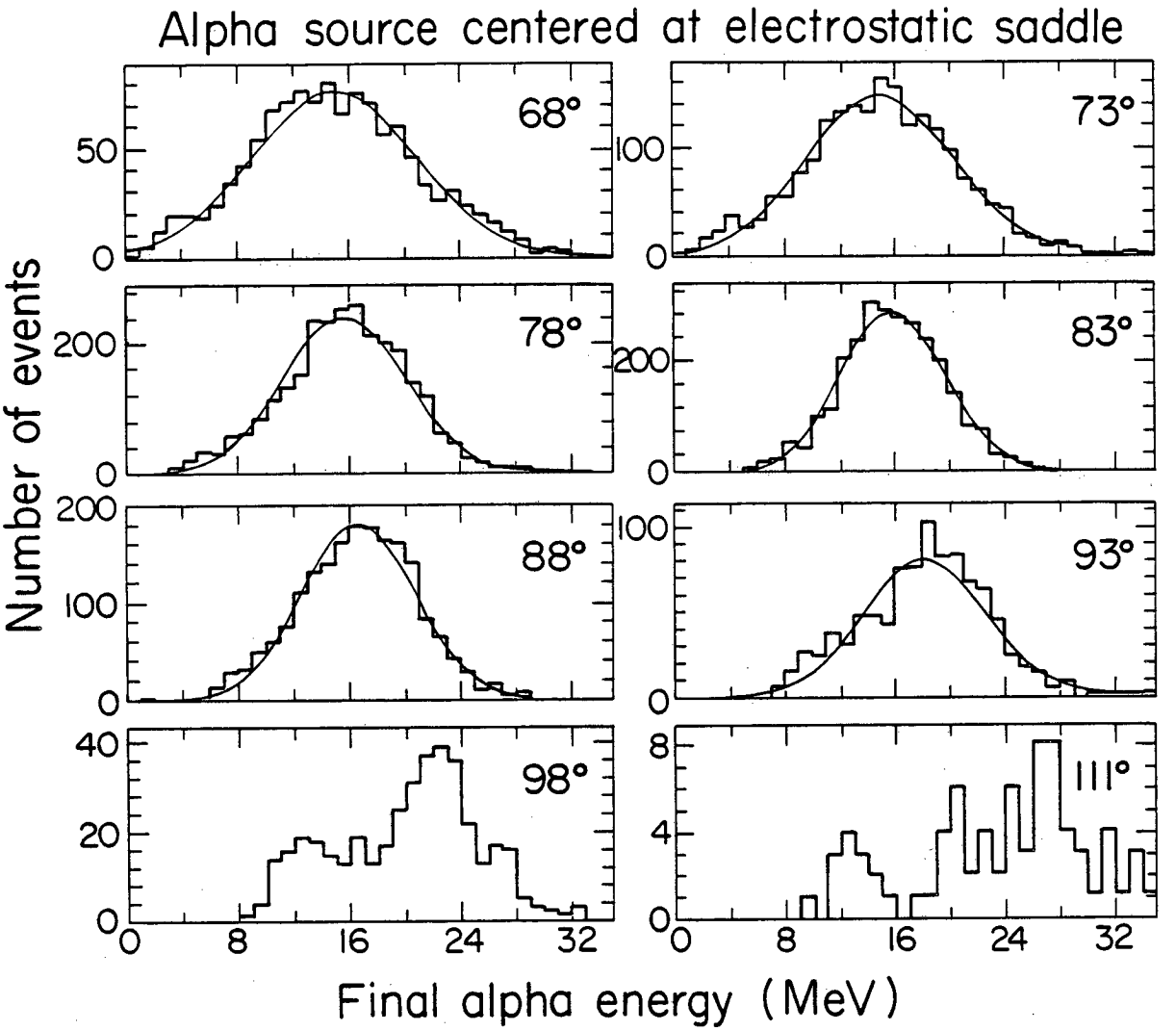
Alpha source centered at electrostatic saddle
68°
73°
78°
83°
88°
93°
98°
111°
Number of events
Final alpha energy (MeV)
XBL 821-4414

Fig. 9

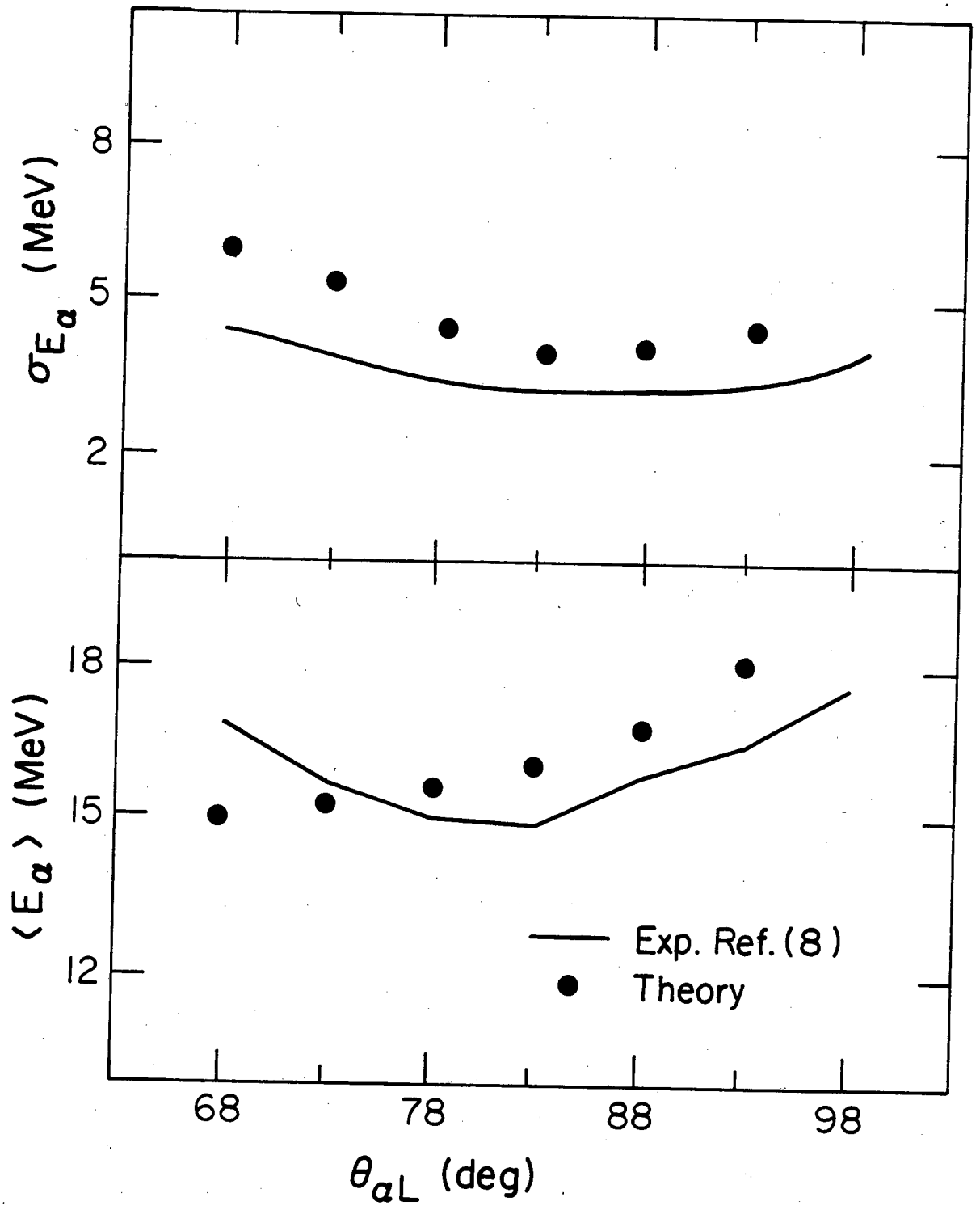

XBL 821-4411

Fig. 10

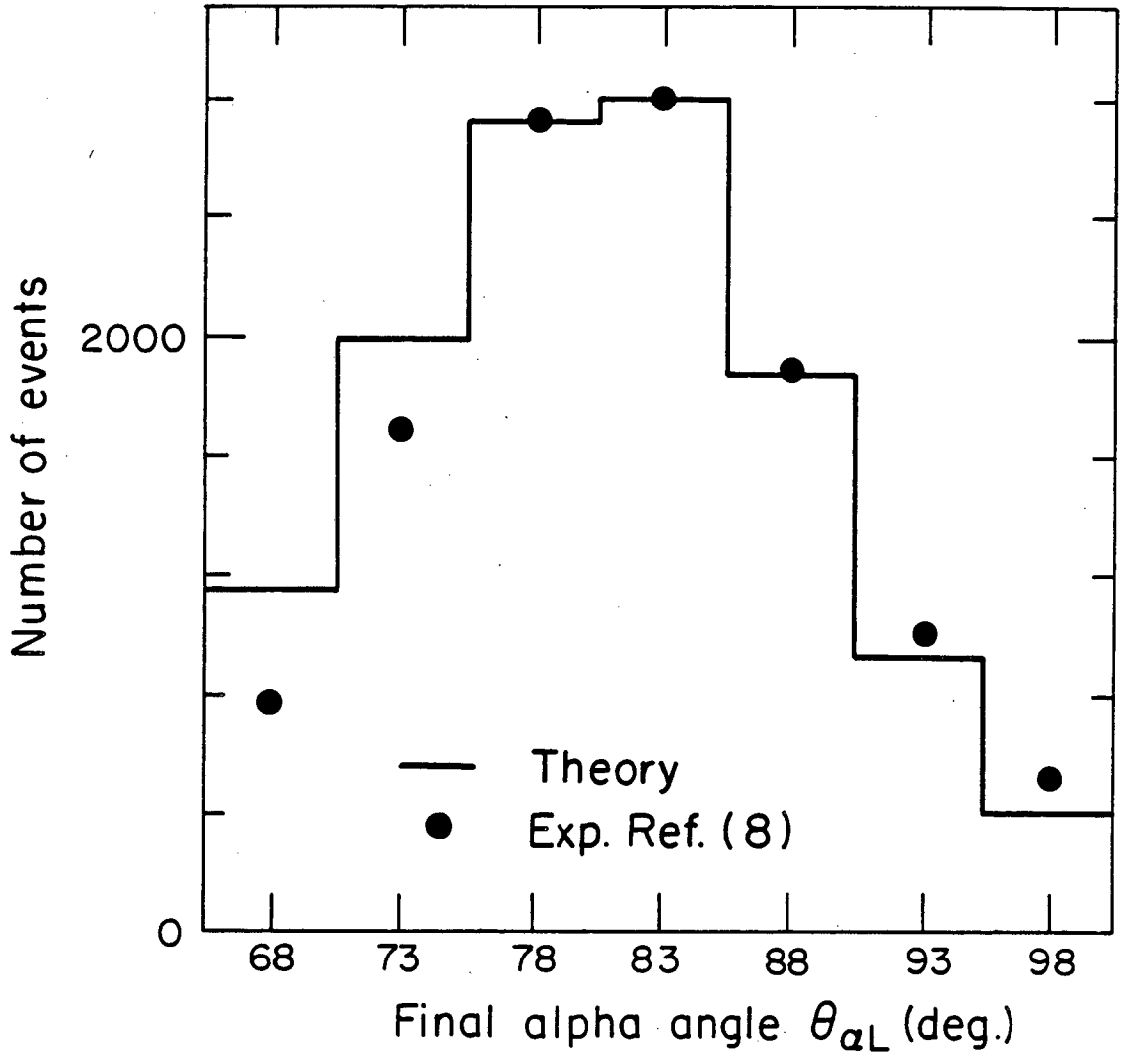

XBL821-4425

Fig. 11

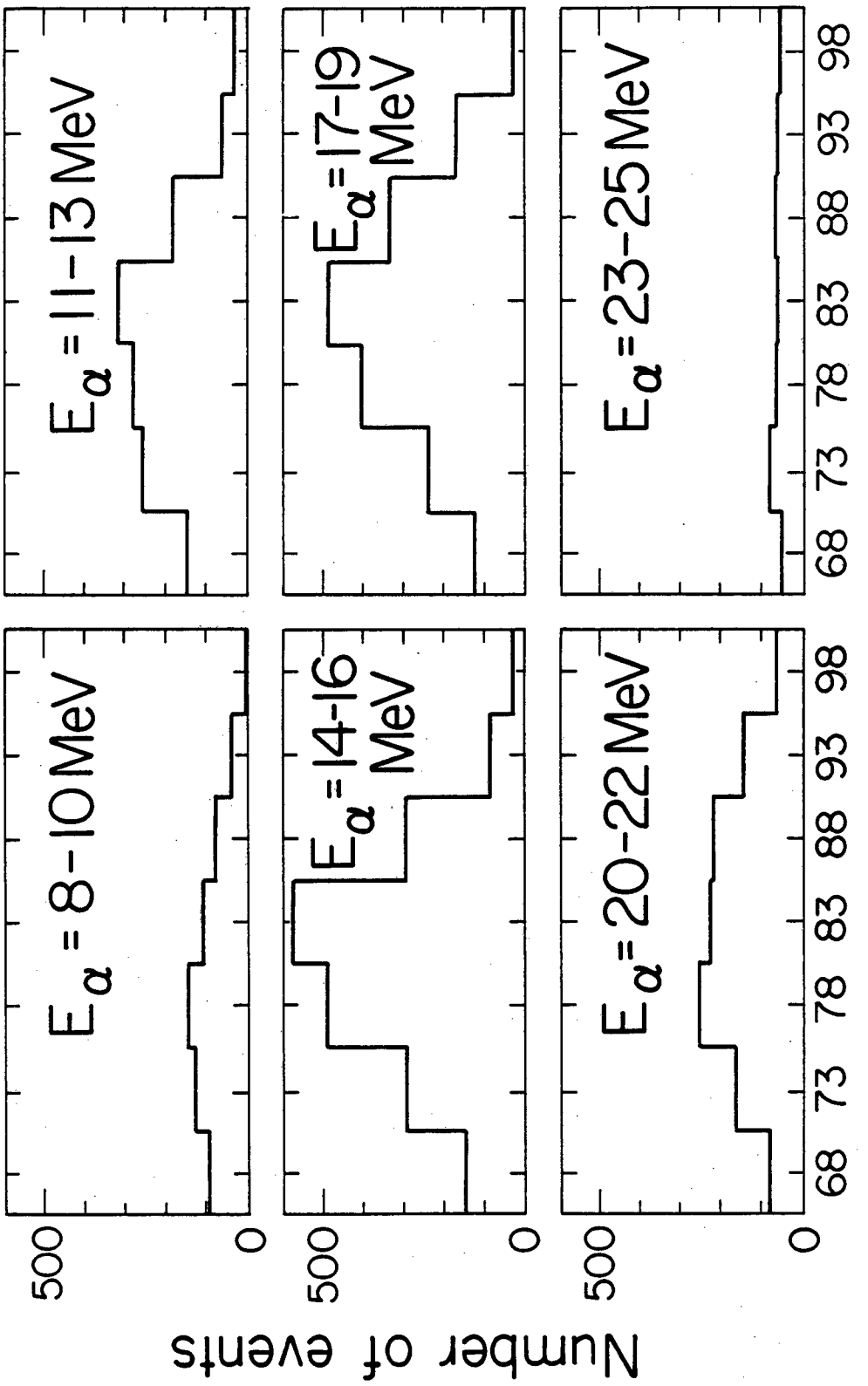

XBL821-4407

Fig. 12

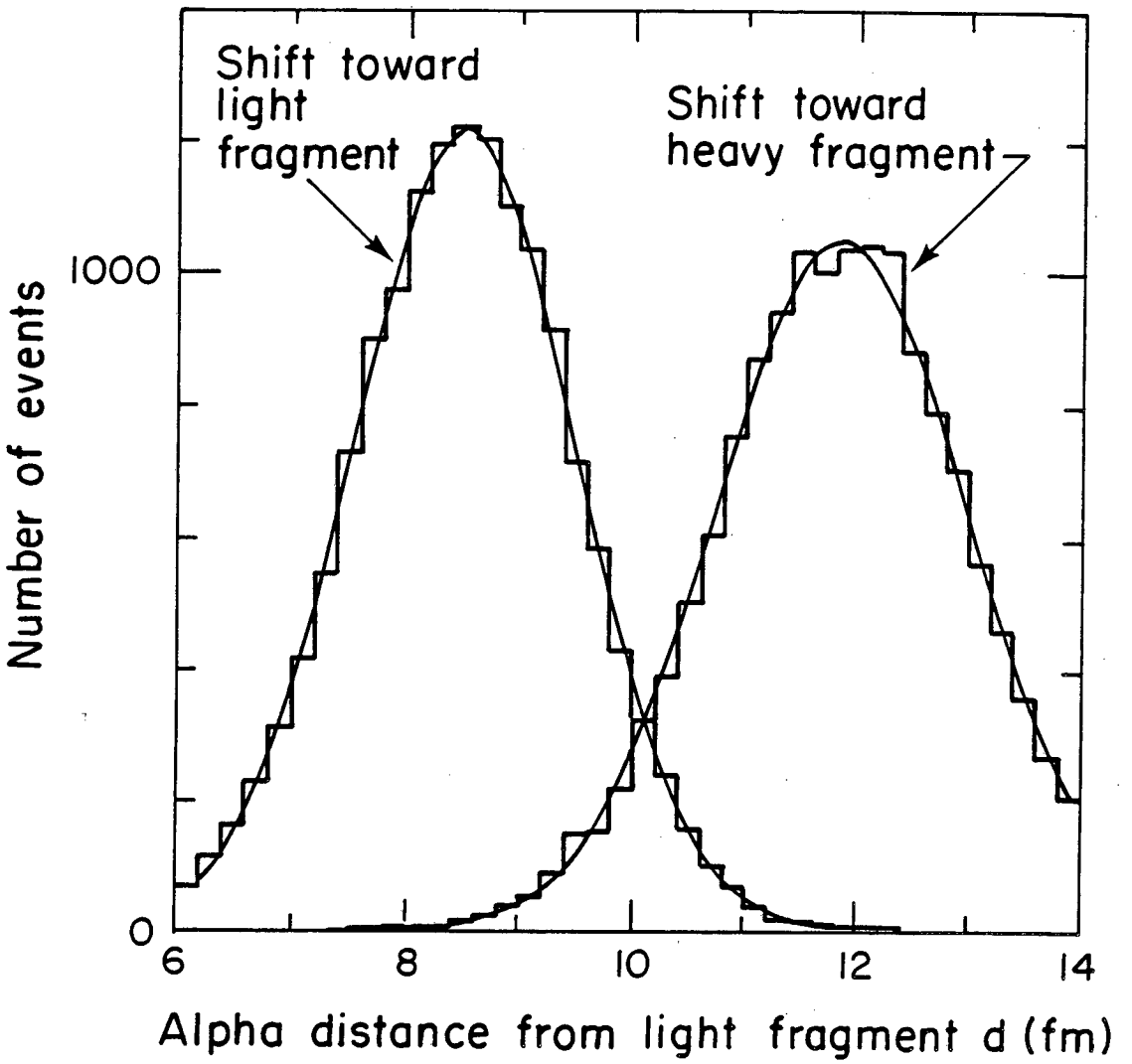

XBL821-4424

Fig. 13

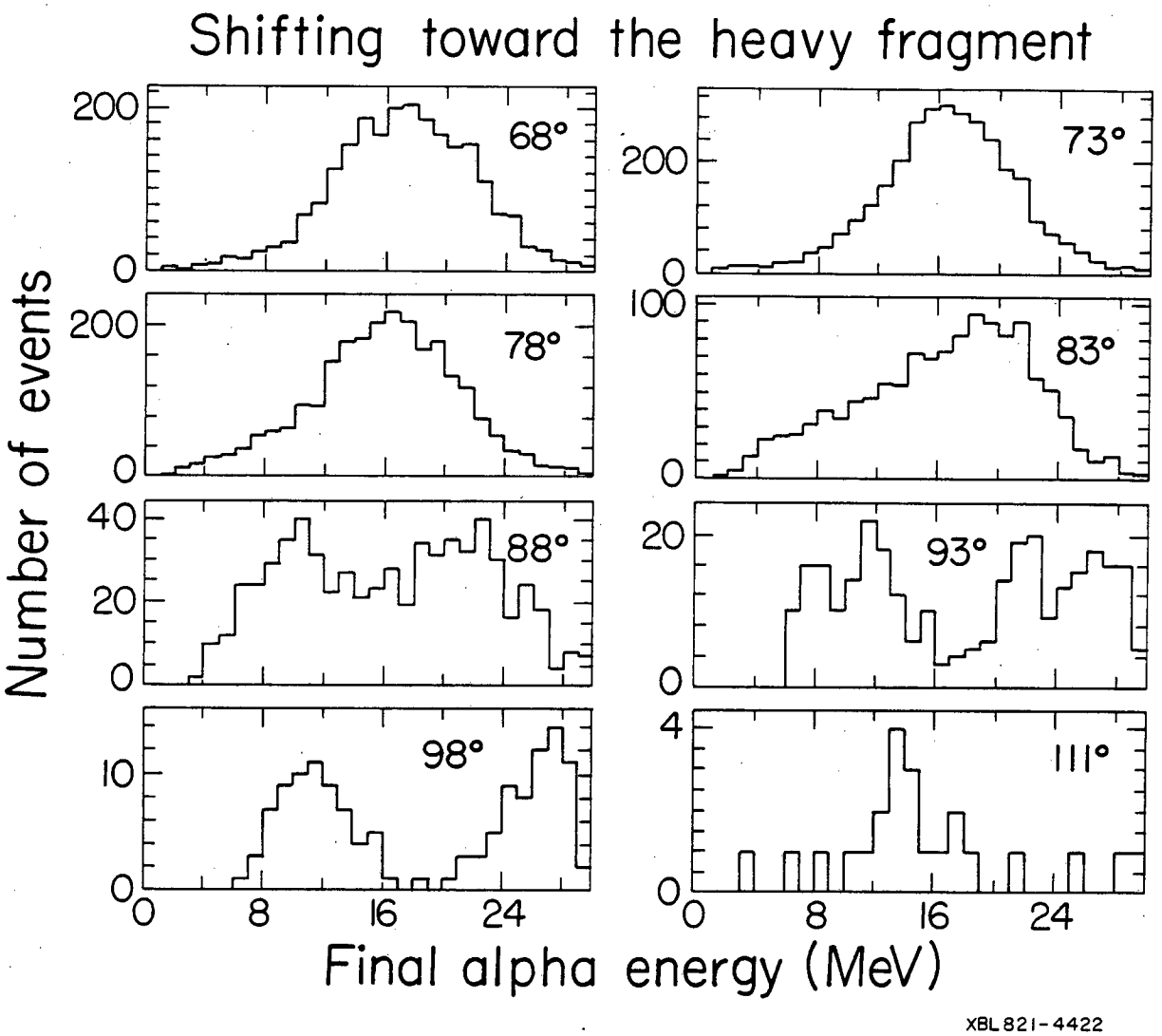
Shifting toward the heavy fragment
Number of events
Final alpha energy (MeV)
68°
73°
78°
83°
88°
93°
98°
111°
200
0
100
40
20
10
4
8
16
24
XBL 821-4422

Fig. 14

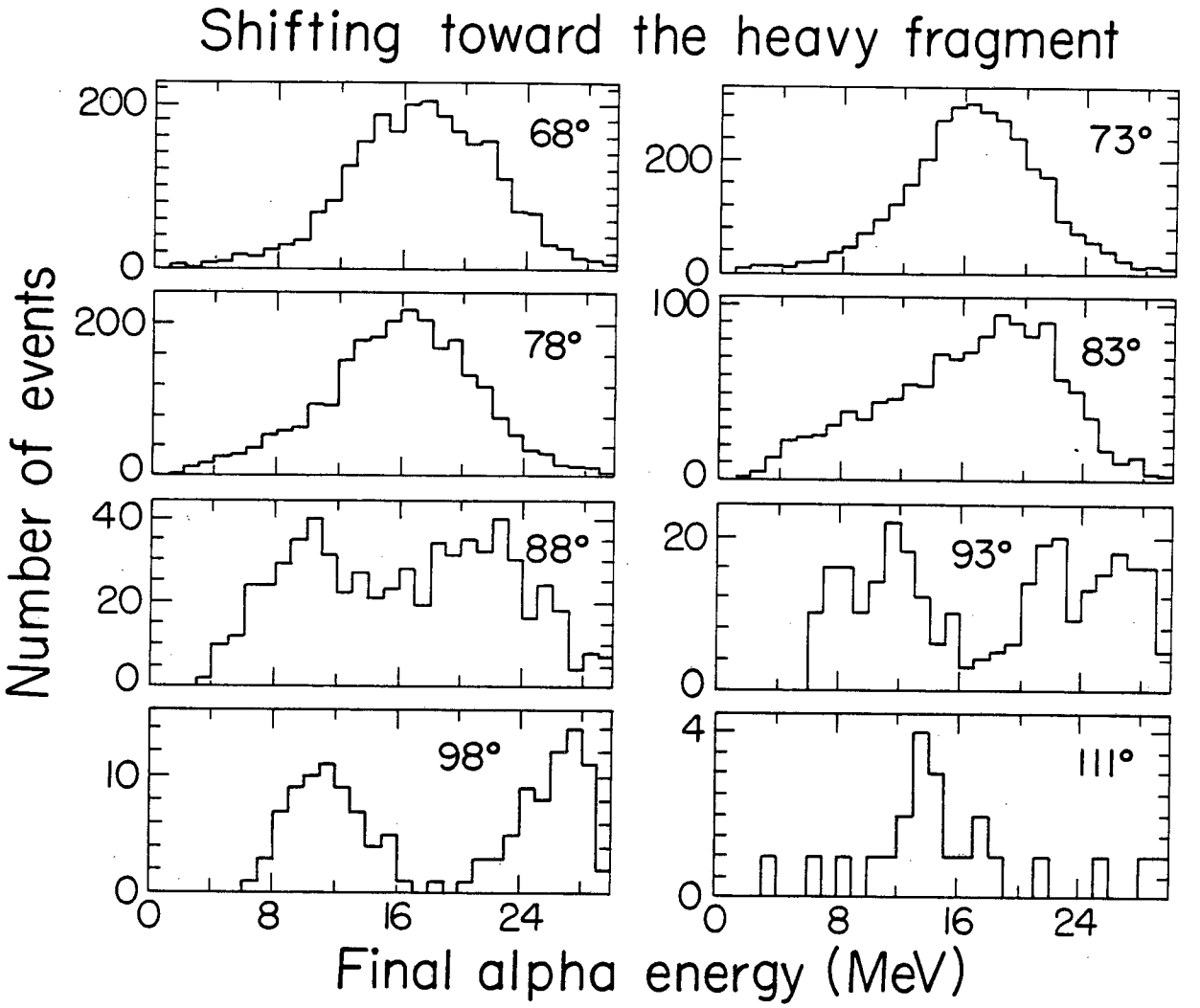
Shifting toward the heavy fragment
Number of events
Final alpha energy (MeV)
68°
73°
78°
83°
88°
93°
98°
111°
200
0
100
40
20
10
4
8
16
24
XBL821-4422

Fig. 15

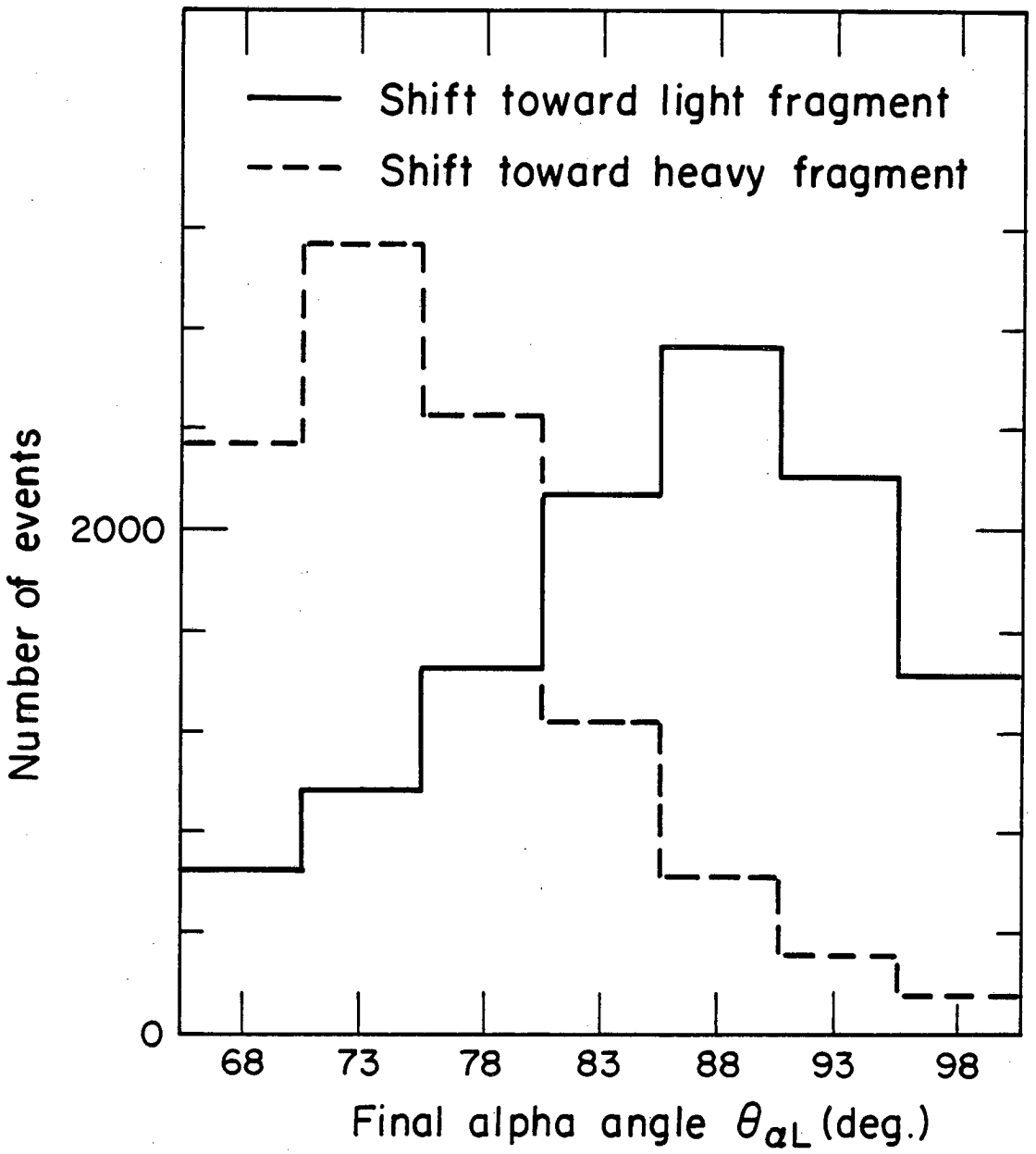

XBL 821-4406

Fig. 16

TECHNICAL INFORMATION DEPARTMENT
LAWRENCE BERKELEY LABORATORY
UNIVERSITY OF CALIFORNIA
BERKELEY, CALIFORNIA 94720